Available online at www.sciencedirect.com
ScienceDirect
Journal of Membrane Science 310 (2008) 174–183
journal of MEMBRANE SCIENCE
www.elsevier.com/locate/memsci

# Enantioselective permeation of racemic alcohol through polymeric membrane

Swapnali Hazarika *

*Chemical Engineering Division, North East Institute of Science and Technology, Jorhat 785006, Assam, India*

Received 28 May 2007; received in revised form 24 October 2007; accepted 28 October 2007
Available online 12 November 2007

**Abstract**

Copolymer of 1,2-bis(2-methyl-1-triethylsiloxy-1-propenyloxy)ethane and dialdehyde have been synthesized by Mukaiyama Aldol polymerization using lipase as the catalyst. The chirality of the polymer was tested by optical rotation and circular dichroism study. The membrane forming ability of this chiral polymer was examined by casting the membrane in three different solvents viz., *N*-methyl-2-pyrilidone (NMP), dimethyl formamide (DMF) and dimethyl acetamide (DMAc) using the phase inversion method and it was found that chiral polymer–NMP membranes formed more uniform and regular surface morphology as was evident from SEM analysis. The enantioselective membranes prepared in the solvents was tested for resolution of racemic alcohol and it was found that NMP is the best solvent for obtaining highest enantioselectivity value. It was also found that the enantioselectivity for adsorption favoured the (*S*)-isomer whereas permeation favoured the (*R*)-isomer which is confirmed from interpretation of the adsorption isotherm by Langmuir model. Accordingly, the enantioselective permeation was caused by suppression of the (*S*)-isomer permeation. Optical resolution of (±)*trans*-sobrerol was achieved by pressure driven permeation through the membrane. The highest enantioselectivity, enantiomeric excess and permeation co-efficient was obtained as 98.59%, 20.42 and 13.627 $m^2\,h^{-1}$, respectively. With an increase in polymer content in the membrane, the permeation rate increases.


*Keywords:* Mukaiyama aldol polymerization; *Trans*-sobrerol; Enantioselective membrane; Polymer–solvent interaction

## 1. Introduction

Optical resolution is a very important separation process, in the field of medicine and agricultural chemicals because of their effectiveness and safety. Optically active compounds are closely related to biological and pharmacological activity and their development as an effective method for producing optically active compound is very important. Conventional optical resolution methods, such as preferential crystallization, chemical modification to a diastereomer with an optical resolution agent, and HPLC with a chiral stationary phase have the common drawback, that is low amount of material treated in one operation. But optical resolution by membrane permeation is very promising because a large amount can be handled in a single operation.

Enantioselectve transport had also been realized for combinations of porous membranes with chiral selector groups, including biomolecules [1,2]. Proteins, such as BSA, immobilized in the pores of UF or MF membranes are presumably the best-studied example [3,4]. The surface modification of a MF membrane with chiral polyglutamates had also yielded membranes with some enantioselectivity [5]. Liquid membranes containing enantiomer recognizing carriers such as chiral crown ether show highly enantioselective permeability [6] but low durability because losses of the liquid and carriers cannot be avoided. Some works on this area are reported by Keurentjes et al. [7].

Research towards solid membranes is focused on two alternatives: the use of chiral or achiral polymers. Optical resolution through solid membrane is expected to be effective for a large amount of racemic compounds. Enantioselective permeation through a polymer membrane was first demonstrated using poly-L-glutamates with amphiphilic *n*-nonylphenoxy-oligoethyleneglycol side chains [8]. In diffusion experiments with tryptophan and tyrosin, selectivities of >8 for the *D* vs. the *L*

* Tel.: +61 376 2370012; fax: +61 376 2370121.
*E-mail address:* shrrljt@yahoo.com.

0376-7388/$ – see front matter © 2007 Elsevier B.V. All rights reserved.
doi:10.1016/j.memsci.2007.10.055

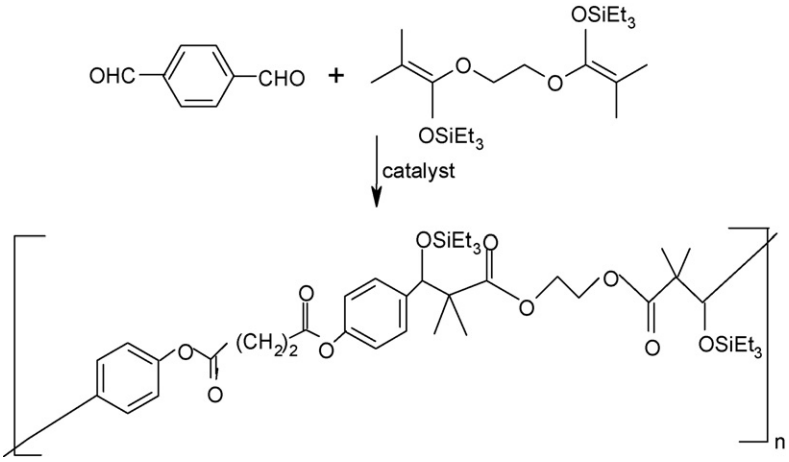


Scheme 1.

isomers had been observed [2]. Aoki et al. and Teraguchi et al. [9–17] reported some chiral membranes for optical resolution. However, they have not yet been used for industrial production. This is because when the membrane showed high selectivity, the permeabilities are too low to be useful. Teraguchi et al. [17] reported polysubstituted acetylenes having chiral pendant groups as optical resolution membrane materials because they have a good membrane forming ability combined with chiral helicity in their main chain.

In this present study, we used solid membrane prepared from a chiral polymer for resolution of racemic compound. For this purpose a chiral polymer have been synthesized by asymmetric aldol polymerization of bis(silyl enol ether) and dialdehyde by Mukaiyama aldol reaction (Scheme 1) where lipase from *C. rugosa* is used as the catalyst, is one of the most important aldol reaction for chiral polymer synthesis (Scheme 1) from which we have also developed a new method for preparation of enantioselective membrane and studied their performance in enantioselective permeation.

## 2. Materials and methods

### 2.1. Chemicals and enzyme

Lipase, *trans*-sobrerol and polysulfone (average mol. wt. 30,000) were supplied by Aldrich Chemical Company, USA, *N*-methyl pyrrolidone (NMP), dimethyl formamide (DMF) and dimethyl acetamide (DMAc) was supplied by SRL-India. Triethylsilane, ethylene glycol dimethacrylate (EGDA), succinoyl chloride, 4-hydroxybenzaldehyde, sodium hydride and solvents were procured from Ranbaxy Fine Chemical Ltd., New Delhi, India.

### 2.2. Analytical methods

IR spectra were obtained on Perkin Elmer, System 2000 FT/IR Infrared spectrophotometer. Data for $^{1}H$ NMR and $^{13}C$ NMR spectra were recorded using BRUKER ADVANCE DPX-300 MHz spectrometer. Chemical shifts were reported in ppm down field from tetramethylsilane with solvent resonance as the internal standard. Optical rotations were determined by JASCO Digital Polarimeter P-1020 using chloroform as the solvent. Circular dichroism study was done by JASCO J810C instrument using chloroform as the solvent at a speed 20 nm/min and wavelength range 240–550 nm. The cell path length was 1 cm with a bandwidth 1 nm at a temperature 20 °C.

Molecular weight of the polymer were determined by measuring percentage of Silicon in the polymer assuming that copolymer formed in the polymerization reaction was of the type $(AB)_n$. Percentage of silicon in the polymer was measured by X-ray fluorescence analysis (XRF) on a SPECTRO XEPOS Benchtop XRF Spectrometer (Version 1.0). Molecular weight of the polymer was obtained as 74,500.

Thermogravimetry (TG) and differential thermogravimetry (DTG) were performed using a Shimadzu Thermal Analyzer 30 at a heating rate of 10 °C/min using $5 \pm 1$ mg of powdered samples in the temperature range from 30 to 500 °C. Differential scanning calorimetry (DSC) was performed on a Perkin Elmer PC series DSC 7 with 3–5 mg of polymer samples weighed in aluminium pans at a heating rate of 10 °C/min. All experiments were carried out in nitrogen atmosphere and the measurement was started as soon as the heat flow in the DSC cell had stabilized.

The HPLC measurements were carried out on a Waters modular system consisting of two 510 pumps, an automated gradient controller, U6K injector and a 486 tunable absorbance detector. The column was CHIRALPAK-WH, 5 μm particle size of the packing material, 250 mm × 4.6 mm i.d. (DAICEL CHEMICAL INDUSTRIES Ltd.). The mobile phase was 0.25 mM aqueous $CuSO_4$. The sample was detected with UV 210 nm and flow rate of 1 mL/min.

### 2.3. Synthesis

As the monomers for the above polymerization reaction are not commercially available, hence it has been synthesized by the procedure reported in literature [18].

#### 2.3.1. Synthesis of dialdehyde (monomer 1)

To a stirred suspension of NaH (0.2 g. 8.33 mmol) in anhydrous THF, 1.02 g (8.33 mmol) of 4-hydroxybenzadehyde was

added under $N_2$ atmosphere, and the mixture was stirred at 0 °C for 1 h. Succinoyl chloride (2.7 ml, 24.5 mmol) was then added and the reaction mixture was stirred for 20 h. After the reaction was completed, a separating funnel separated the organic layer and the residual aqueous layer was extracted twice with ethyl acetate. The combined organic layer was dried over $Na_2SO_4$. The mixture was then filtered and concentrated in a rota vapour to give the solid product and recrystallized the crude product from hexane/EtOAc (yield 22.45%). $^1$H NMR ($\delta$ in ppm from TMS in $CDCl_3$): 3.05 (br s, 4H), 7.30 (d, 4H), 7.93 (d, 4H), 10.00 (s, 2H), $^{13}$C NMR: 29.18, 122.23, 131.20, 134.21, 155.13, 170.01, 190.71; IR (KBr, cm$^{-1}$) 2840, 2746, 1752, 1696, 1596, 1317, 1205, 1136, 924, 834, 794, 675, 508.

#### 2.3.2. Synthesis of 1,2-bis(2-methyl-1-triethylsiloxy-1-propenyloxy)ethane (monomer 2)

Ethylene glycol dimethacrylate (2 g (10.4 mmol)) and 2.9 g (24.9 mmol) of triethylsilane was mixed with 200 mg of Wilkinson catalyst ($Rh(PPh_3)_3Cl$) and heated to 60 °C and stirred for 10 min. After fractional distillation under reduced pressure monomer 2 was obtained as a colourless oil (yield ~80%). $^1$H NMR ($\delta$ in ppm from TMS in $CDCl_3$): 0.73 (q, 12H), 0.99 (t, 18H), 1.54 (s, 6H), 1.58 (s, 6H), 3.87 (s, 4H); $^{13}$C NMR: 4.9, 6.6, 16.4, 16.9, 67.5, 91.7, 148.4.

#### 2.3.3. Synthesis of polymer

*2.3.3.1. Lipase catalyzed polymerization reaction. Candida rugosa* lipase (20 mg/ml) was mixed with toluene solution at room temperature. After stirring for 30 min the solvent was removed and the resulting white solid was suspended in 10 ml $CH_2Cl_2$. Then a $CH_2Cl_2$ solution of 0.802 mmol/L of monomer 1 and 0.726 mmol/L of monomer 2 was added successively. The resulting mixture was stirred for 70 h at 30 °C. After removal of the solvent, the THF solution of the crude product was poured into MeOH/$H_2O$ (2:1). The precipitated polymer was filtered and dried *in vacuo* (yield 38%).

### 2.4. Preparation of membrane

The membrane was cast by so-called phase inversion method from a solution consisted of polysulfone, chiral polymer, polyethylene glycol as organic additive in three different solvents viz., dimethyl formamide (DMF), dimethyl acetamide (DMAc) and *N*-methyl-2-pyrrolidone (NMP). Composition of the casting solution with different amount of chiral polymer is reported in Table 1. All the components were stirred at 45 °C until a homogeneous solution was achieved. Film was cast on a glass plate with a Doctor's knife while the solution mixture was at that temperature by the phase inversion method. The solvent was evaporated in an oven at 80 °C for 2 h. Gelation was done in ice-cold water for 24 h.

### 2.5. Characterization of membrane

The enantioselective membrane was characterized for pore size and surface morphology through microscopic observation. Microscopic observation is carried out by a scanning electron microscope (LEO 1430VP, UK), which directly provides the visual information of the membrane morphology such as pore shape, size, their distribution and density. Computerized analysis of SEM image is a standard and widely used method for the investigation of perforated materials [19,20]. In the present study, Image J Launcher Broken Symmetry Software is used to measure the morphological parameters such as pore size and hence the pore size distribution of each membrane. For this, SEM photographs are taken at different locations of the same membrane sheet from which the pore sizes are measured. This gives us the information regarding the number of pores in different pore size ranges from which percentage of pores in various pore size ranges can be calculated. Plotting percentage of numbers of pores against pore size gives the pore size distribution curve. In this study, average (or mean) pore radius is considered as a substitution for the true pore radius. The mean pore radius is calculated by

$$r_m = \left( \frac{\sum n_i r_i^2}{\sum n_i} \right)^{1/2} \quad (1)$$

where $r_m$ is the mean pore radius (μm); $r_i$ is the radius of the pores of different size (μm) and $n_i$ is the number of pores of radius $r_i$.

Total pore area is calculated from the knowledge of the mean pore radius and the total number of pores within a known

Table 1
Physical properties of chiral membrane

| Solvent | wt.% of chiral polymer | Membrane thickness (μm) | Pore diameter (nm) | Surface porosity (ε%) | Pure water permeability ($\times 10^{-6}$ g m m$^{-2}$ h$^{-1}$) |
|---|---|---|---|---|---|
| NMP | 2.0 | 130 | 0.01 | 1.15 | 4.46 |
| | 7.5 | 131 | 0.05 | 2.23 | 5.09 |
| | 10.0 | 135 | 0.25 | 2.24 | 5.59 |
| DMAc | 2.0 | 12 | 0.03 | 0.27 | 6.89 |
| | 7.5 | 14 | 0.01 | 0.30 | 6.99 |
| | 10.0 | 17 | 0.22 | 0.59 | 7.29 |
| DMF | 2.0 | 76 | 0.23 | 0.19 | 3.10 |
| | 7.5 | 75 | 0.21 | 0.22 | 3.11 |
| | 10.0 | 78 | 0.32 | 0.34 | 3.19 |

Polysulfone = 15 wt.% and additive = 1 wt.%.

membrane area. Assuming similar pore distribution for the entire membrane sheet, the surface porosity ($\varepsilon$) is calculated as follows [21]:

$$\varepsilon = \frac{\sum(n_i \pi d_i^2)}{4A} \tag{2}$$

where $A$ is the total membrane area ($\mu m^2$) and $d_i$ is pore diameter ($\mu m$). The total number of pores per unit membrane area gives the pore density:

$$\text{pore density}\,(\%) = \frac{\sum n_i}{A} \tag{3}$$

The thickness of the prepared membranes is also calculated from SEM photographs of the cross-section of the membranes using standard technique reported in literature [22]. Such photographs also provide us with the information regarding the structure and the presence of any micro voids in the sub layer of the membrane sheets. Some SEM photographs of chiral membranes obtained in various solvents are shown in Fig. 1.

Microscopic observation gives an approximate value of pore size, and the values were confirmed by modified bubble point method [23], which is originally developed by Capanelli et al. [24]. In this method the water saturated *iso*-butanol ($\delta = 1.7$ dynes $cm^{-1}$) was used to displace water in prewetted membranes at pressure 1 and 1.5 $N/m^2$. The pore radii ($r$) and the number of pores ($n$) were calculated using equation:

$$r = 2\delta \cos\frac{\theta}{P_2} \tag{4}$$

and

$$n = \left[J_2 - \frac{J_1 P_2}{P_1}\right] \frac{8\eta 1}{\pi P_2 r^4} \tag{5}$$

where $\delta$, $\theta$, $n$, $\eta$, $l$, $P$ and $J$ are the water/water saturated polymer contact angle, number of pores, viscosity, pore length (membrane skin layer thickness), applied pressure and the permeate flow rate, respectively.

Pure water permeability for all membranes was measured in a membrane cell of standard design. The membranes with effective area of 28.3 $cm^2$ were set in the test cell and the pure water permeability test was carried out by applying $4.84 \times 10^{-2}$ $N/m^2$ pressure to the feed side. The quantity of water permeated through the membrane was measured as permeation rate (g m $m^{-2}$ $h^{-1}$). Some physical properties such as membrane thickness, pore diameter, surface porosity and pure water permeability of chiral membranes are shown in Table 1.

### 2.6. Adsorption experiment

For adsorption experiment, 20 ml of aqueous solution of racemic compound was contacted with pre-weighed chiral membrane in three different solvents viz., NMP, DMAc, DMF containing different amount of chiral polymer between 0.05 and 0.2 g and was placed in a thermo stated shaker maintained at $25 \pm 0.5$ °C. Preliminary run showed that adsorption equilibrium was achieved after 6 h of contact time for aqueous solution

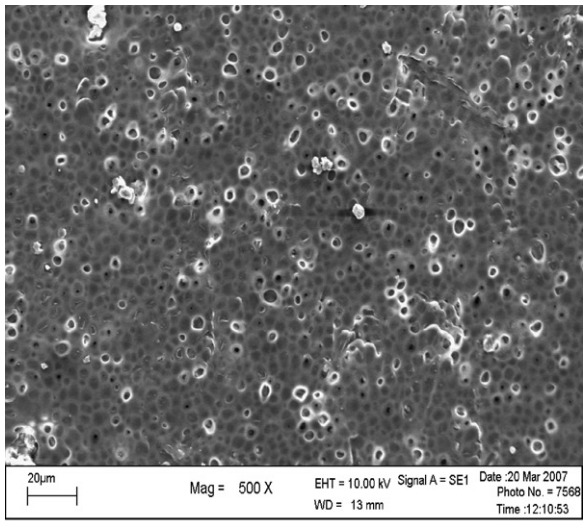


(a)

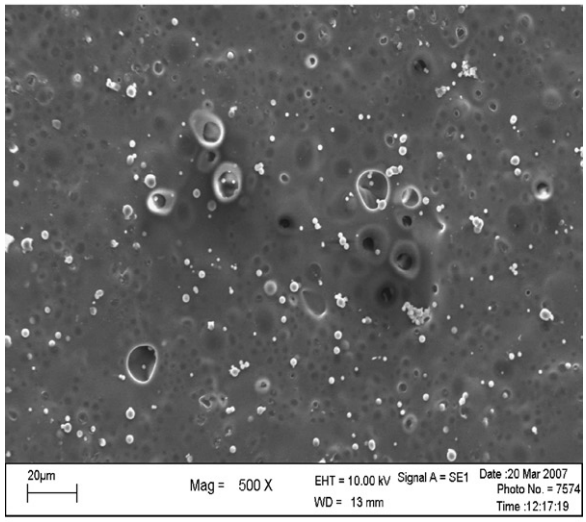


(b)

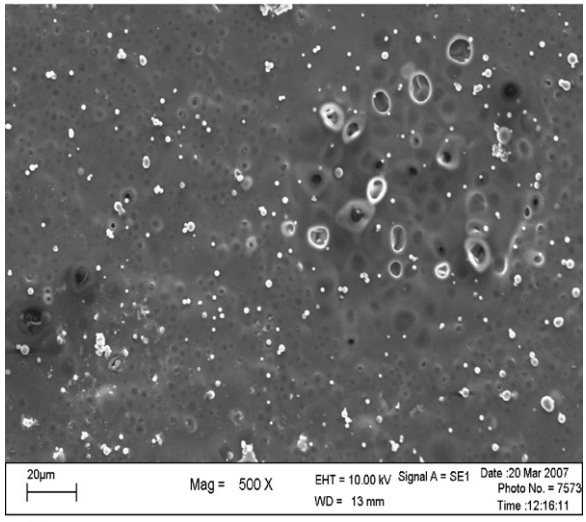


(c)

Fig. 1. (a) SEM photograph of enantioselective membrane in NMP. (b) SEM photograph of enantioselective membrane in DMAc. (c) SEM photograph of enantioselective membrane in DMF.

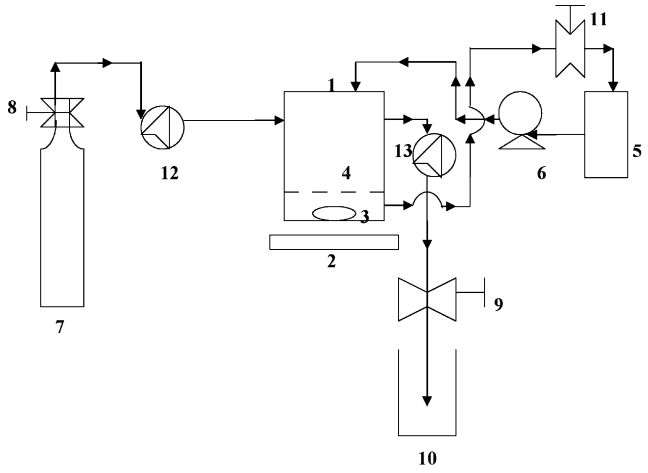


Fig. 2. Flow diagram of permeation experiment. 1, membrane cell; 2, magnetic stirrer; 3, magnetic capsule; 4, membrane; 5, feed tank; 6, peristaltic pump; 7, $N_2$ gas; 8, gas valve; 9, gas valve; 10, water vessel; 11, sample collecting valve; 12, pressure guaze; 13, pressure guaze.

of *trans*-sobrerol and accordingly, all equilibrium experiments were conducted at 7–8 h. The initial concentration of *trans*-sobrerol was taken between 2 and 8 mM. The samples were collected at a regular interval of time till the equilibrium is achieved and analyzed by HPLC chiral column. The amount of *R*- or *S*-isomer adsorbed per gm of chiral polymer $q$ (mmol $g^{-1}$) was calculated as $q = V_1 \Delta C/W_1$ where $\Delta C$ is the change in solute concentration (mM) $V_1$ is the solution volume (l) and $W_1$ is the weight of adsorbent (g).

### 2.7. Permeation experiment

A disproportionate two-compartment membrane cell (Fig. 2) whose compartments volumes on the feed side and permeate side were 150 and 20 ml, respectively was used. The polymeric membrane was placed between the compartments with silicone–rubber packing and the cell was connected with a reservoir of 500 ml. The aqueous solutions of the model compound was stirred continuously and circulated by peristaltic pump that was connected to the reservoir. The area of the membrane was 28.3 $cm^2$ and the transmembrane pressure of the experiment was 0.95 $N/m^2$. The sample solutions were collected from the permeate side after a permeation period and analyzed by HPLC chiral column.

### 2.8. Calculations

The transport rate for both *S*- and *R*-enantiomer through chiral activated membrane, and the membrane enantioselectivity were estimated. The transport rate is expressed in terms of recovery percentage ($R$), which is calculated as the ratio of *S*- or *R*-isomer concentration in the permeate phase at any time $t$ ($C_{pt,E-}$) to the initial *R*- or *S*-isomer concentration in the feed phase ($C_{fo,E-}$):

$$R = \left(\frac{C_{pt,E-}}{C_{fo,E-}}\right) \times 100 \tag{6}$$

The *R*-values are corresponding to the sum of the recovery percentage of the two enantiomers.

The normalized quantity ($Q_c$ (g m $m^{-2}$)) was calculated from the following equation [17]:

$$Q_c = \frac{W_2 L}{A} \tag{7}$$

where $W_2$ is the weight of solute after a permeation period (in g) which was calculated from HPLC data, $L$ and $A$ are the thickness and area of the membrane. The permeation rate ($P_c$ (g m $m^{-2}$ $h^{-1}$)) for racemic compound was estimated from the slope of the $Q_c$ vs. permeation time (min) plot. The permeability co-efficient ($P$ in $m^2$ $h^{-1}$) was calculated by dividing $P_c$ by the difference in the concentration between the feed and permeate sides.

The enantioselectivity of the process is given in terms of alpha values ($\alpha$) as well as in terms of enantiomeric excess (ee). Alpha values were calculated by the following formula [25]:

$$\alpha = \frac{J_{t,R-}}{J_{t,S-}} \tag{8}$$

where $J_{t,S-}$ and $J_{t,R-}$ apply for the fluxes of *S*-enantiomers and *R*-enantiomers (g m $m^{-2}$ $h^{-1}$), respectively, at time $t$. Flux can be calculated as [26]

$$J_{t,S-} = -\frac{V_2\, \Delta C}{A\, \Delta t} \tag{9}$$

where $V_2$ is the volume of feed or permeate phase, $\Delta C$ the concentration variation in the corresponding aqueous solutions at the time increment $\Delta t$ and $A$ is the membrane area.

The enantiomeric excess corresponds to the ratio of the difference between the concentration of both enantiomers in the permeate phase to the total amount of both enantiomers transported at any time and was calculated using the following equation [27]:

$$\text{ee} = \frac{(C_{t,S-}) - C_{t,R-}}{(C_{t,S-}) + C_{t,R-}} \times 100 \tag{10}$$

where $C_{t,S-}$ and $C_{t,R-}$ correspond to the concentration of the *S*-enantiomer and *R*-enantiomer at any time $t$, respectively.

## 3. Results and discussions

### 3.1. Optical properties of the polymer

The important factors determining optical activity in synthetic polymers are (i) the chirality of the repeat units and (ii) the presence of a secondary structure, such as helix [28]. The extent of contribution of the each factor to the optical rotation of the polymer may be determined from the dependence of the mean residue rotation (rotation per repeat unit) on molecular weight. For no contribution from a secondary structure, the observed mean residue rotation will be independent of molecular weight. However, in general, the optical rotation value may increase by about 1–500° $dm^{-1}$ $g^{-1}$ $cm^3$ on transforming a monomer into polymer [29], which is because of the presence of secondary structure in the polymer.

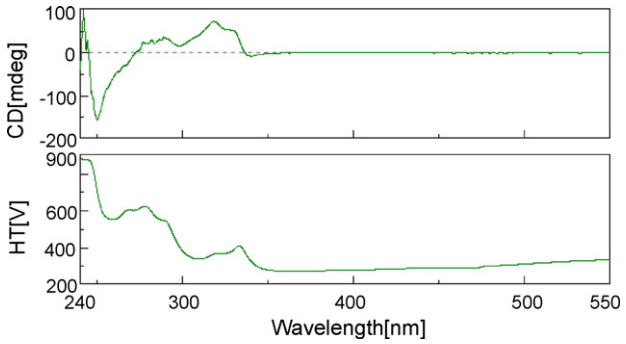


Fig. 3. Circular dichrosm spectra for chiral polymer.

The optical rotation ($[\alpha]^{25}$, $c = 1$ in $CHCl_3$) values of our chiral polymer was observed to be +9.8. The dihedral angle, which is the main factor controlling the optical activity of biaryl compounds, is not expected to depend on the $M_w$ of the polymer. The facts that the observed rotation is $M_w$ dependent [30] suggest that the optical rotations are influenced by some secondary structure, perhaps in addition to the influence of the chirality of the repeat unit. The high optical rotations observed and their dependence on $M_w$ led us to conclude that the cyclopolymers adopt an ordered conformation, possibly a helix [28].

From the optical rotation value, the existence of secondary structure cannot be inferred in case of copolymer, but the same can be obtained using circular dichrosm (CD) measurement. Fig. 3 shows the circular dichrosm spectra of the chiral polymer. The spectrum shows a negative cotton effect at 245 nm and a positive one at 232 nm, respectively. The polymer showed large values of the molar ellipticity [31] in the UV region, which is assigned to adsorption by the main chain, a fact leading to the conclusion that the polymer has one handed helical main chain, similar to the results as reported by Teraguchi and Masuda [15].

### 3.2. Thermal behaviour of chiral polymer

During the use of this type of chiral polymers, the stability of the chiral polymer against thermal stress is of great importance. Hence, thermo gravimetric analysis was carried out under nitrogen atmosphere at a heating rate of 10 °C/min. The decomposition curve of the chiral polymer is shown in Fig. 4 wherein the derivative curve is also shown. The results of TGA study on the chiral polymer under nitrogen supports apparent two-step decomposition. The first step decomposition starts above 160 °C with the second step decomposition starting above 280 °C. This corresponds to the random scission within the polymer chain. As the decomposition temperature is high enough, it can tolerate the applied thermal stress during the usage. Furthermore, when the chiral polymer degrades, it leaves nearly no residue at and above 450 °C. To make an accurate quantitative prediction on thermal degradation of chiral polymers, the information of the underlying chemical mechanism is insufficient [32]. Therefore, the development of a molecular level understanding of the thermal degradation of chiral polymers is an increasingly important area of research.

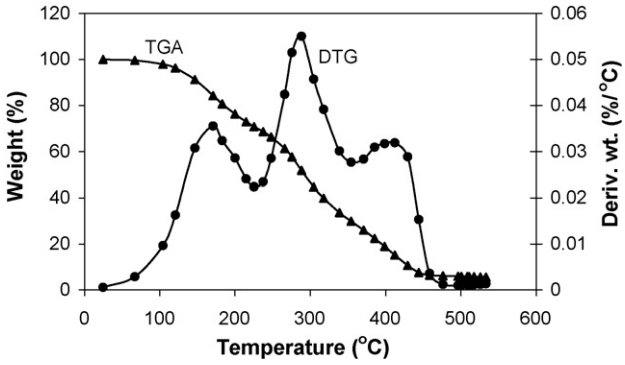


Fig. 4. Thermogravimetric and differential thermogravimeric curve of chiral polymer.

DSC measurements of the polymer were carried out at a heating rate of 10 °C min$^{-1}$ in a nitrogen atmosphere. Melting endothermic peak was obtained at 85–266 °C for this chiral polymer (Fig. 5). The melting point and the heat capacity of the polymer was determined from the endothermic peaks and was found to be 260 °C and 1.2 J/g °C, respectively. The chiral polymer exhibits a single peak indicating the formation of random copolymer.

### 3.3. Effect of casting solvent on the surface morphologies of enantioselective membrane

The surface morphology of chiral membrane has been studied in three different solvents viz., DMAc, DMF and NMP from polymer–solvent interaction point of view. In a good solvent the polymer is unfolded, obtaining to the maximum extent the more favourable polymer–solvent interactions as reported by Guan et al. [33]. The relative strength of polymer–solvent interactions determines the properties of casting solvent and presumably the morphologies and properties of the final membranes [34].

The affinity of solvents can be estimated by introducing the "solubility parameter" $\delta$ which is defined as the square root of the cohesive energy density and describes the strength of attractive force between molecules. Polymer–solvent interactions ($\delta$) in

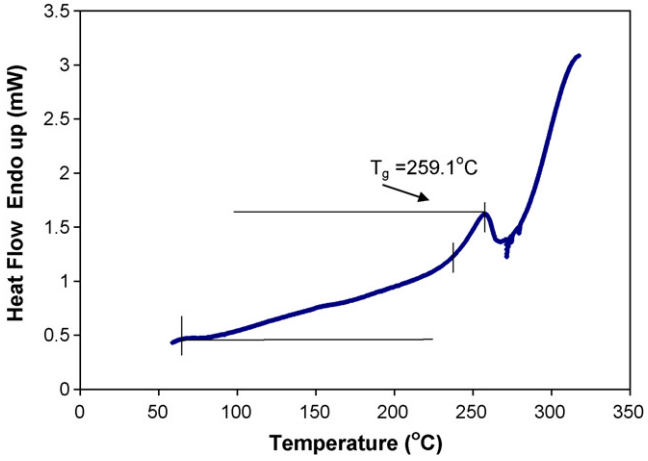


Fig. 5. DSC thermogram for chiral polymer.

Table 2
Hansen solubility parameters for selected solvents and the difference in solubility parameters between solvent and chiral polymer

| Solvent | $\delta_d$ (MPa)$^{1/2}$ | $\delta_P$ (MPa)$^{1/2}$ | $\delta_h$ (MPa)$^{1/2}$ | $\delta$ (MPa)$^{1/2}$ | $\Delta$ |
|---|---|---|---|---|---|
| NMP | 16.4 | 13.2 | 9.4 | 23.05 | 4.29 |
| DMAc | 17.8 | 11.1 | 8.7 | 22.70 | 3.20 |
| DMF | 17.4 | 10.5 | 6.8 | 21.43 | 2.11 |
| Chiral polymer | 16.2 | 10.2 | 10.5 | 21.83 | – |

polymer solution have been evaluated as the difference between solubility parameters of polymer and solvents [33]. $\delta$ can be obtained as

$$\delta^2 = \delta_d^2 + \delta_p^2 + \delta_h^2 \quad (11)$$

where $\delta_d$ is the dispersive force, $\delta_p$ is the permanent dipole–dipole interaction and $\delta_h$ hydrogen bonding forces.

The difference in Hansen solubility parameters between solvent and polymer was calculated using equation:

$$\Delta = \sqrt{(\delta_{P,d} - \delta_{S,d})^2 + (\delta_{P,p} - \delta_{S,p})^2 + (\delta_{P,h} - \delta_{S,h})^2} \quad (12)$$

where P and S represent the polymer and solvent and d, p and h indicate dispersive, polar and hydrogen bonding components of Hansen solubility parameters.

The Hansen solubility parameter of three solvents and the $\Delta$ values between solvent and chiral polymer are shown in Table 2. The smaller the difference between the solubility parameters of polymer and solvent, the stronger the polymer–solvent interaction. Compared to other two membranes, the stronger is the polymer solvent interaction between NMP and chiral polymer results in more regular surface morphology of chiral polymer–NMP membrane, which supports the hypothesis that reported by Guan et al. [33].

### 3.4. Adsorption isotherm

Assuming reversible one-to-one complexation of chiral moiety and enantiomers, complexation can be described analogously to Langmuir adsorption isotherm. Considering adsorption equilibrium, Langmuir has derived the classical equilibrium isotherm for localized nonlinear monolayer adsorption [35]. Accordingly single enantiomer complexation can be described as

$$q_{nR} = \frac{X_{mR} K_R C_{eR}}{1 + K_R C_{eR}} \quad (13)$$

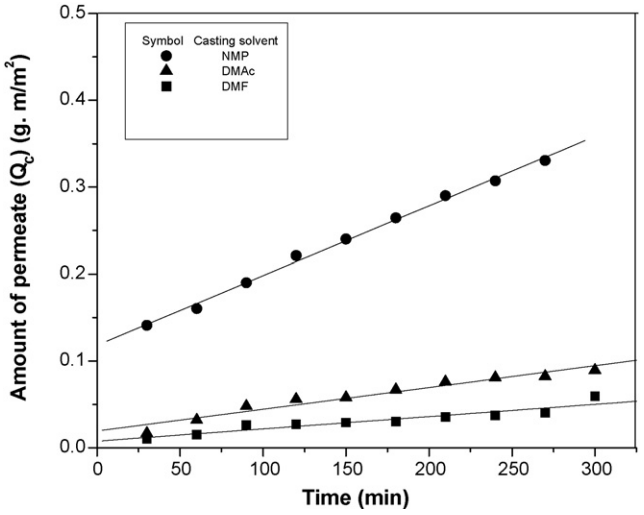


Fig. 6. Plots of quantity of permeated ($Q_c$) vs. permeation time through enantioselective membrane prepared in different solvents.

and

$$q_{nS} = \frac{X_{mS} K_S C_{eS}}{1 + K_S C_{eS}} \quad (14)$$

where $K$ (mM$^{-1}$) is the Langmuir affinity constant, $C_e$ and $q_n$ (mM) are the equilibrium concentration of bulk and bound enantiomers, respectively. The indices R and S refer to the *R* and *S* enantiomers, respectively. The Langmuir saturation constant $X_m$ (mM) is the maximum attainable concentration of bound enantiomer.

Table 3 shows the value of isotherm parameters estimated by non-linear regression analysis. Comparing the co-efficient of determination ($R^2$) of the models it appears that the isotherm provides the most satisfactory representation with the experimental data of *S*-isomer in chiral polymer–NMP membrane.

### 3.5. Enantioseloective permeation

#### 3.5.1. Effect of solvent

The normalized quantity ($Q_c$) of permeated (*R*)-isomer of *trans*-sobrerol vs. permeation time through chiral polymeric membranes in NMP, DMAc and DMF is shown in Fig. 6, from which it may be evident that the chiral membrane prepared by using NMP as the solvent gives the highest permeation rate for (*R*)-isomer of *trans*-sobrerol. Probable reason is higher selectivity in NMP as indicated by Hansen solubility parameters

Table 3
Parameter values for the adsorption isotherm of *R*- and *S*-isomer of *trans*-sobrerol on chiral polymeric membrane (Langmuir model)

| Solvent | $q_{nR} = \frac{X_{mS} K_S C_{eS}}{1+K_S C_{eS}}$ [a] | | | $q_{nS} = \frac{X_{mR} K_R C_{eR}}{1+K_R C_{eR}}$ [b] | | |
|---|---|---|---|---|---|---|
| | $K_S$ (mM$^{-1}$) | $X_{mS}$ (mM) | $R^2$ | $K_R$ (mM$^{-1}$) | $X_{mR}$ (mM) | $R^2$ |
| NMP | 9.6284 | 0.7623 | 0.9133 | 1.1745 | 3.0293 | 0.9951 |
| DMAc | 3.9205 | 1.7602 | 0.9922 | 0.3245 | 1.3629 | 0.9975 |
| DMF | 0.9394 | 2.0552 | 0.9958 | 0.0369 | 1.4457 | 0.9862 |

[a] *S*-Isomer.
[b] *R*-Isomer.

Table 4
Enantioselective permeation of *trans*-sobrerol through chiral membrane (6 h experiment)

| Solvent | Concentration of *trans*-sobrerol (mM) | Permeability co-efficient ($\times 10^{-1}$ m$^2$ h$^{-1}$) | Enantioselectivity ($\alpha$) | Enantiomeric excess (ee%) |
|---|---|---|---|---|
| NMP | 2 | 5.08 | 5.03 | 66.82 |
| | 4 | 9.37 | 13.56 | 88.03 |
| | 6 | 16.57 | 18.00 | 97.56 |
| | 8 | 136.27 | 20.42 | 98.59 |
| DMAc | 2 | 1.83 | 2.03 | 32.32 |
| | 4 | 2.95 | 4.11 | 37.09 |
| | 6 | 3.31 | 4.68 | 48.00 |
| | 8 | 9.23 | 4.90 | 49.46 |
| DMF | 2 | 1.25 | 1.00 | 12.45 |
| | 4 | 1.72 | 1.43 | 14.21 |
| | 6 | 1.91 | 1.87 | 16.77 |
| | 8 | 2.43 | 2.09 | 19.22 |

the values of which are given in Table 2. From Table 4 it may be inferred that both ee and *P* increases with solute concentration. While the increase in *P* with solute concentration may be attributed to the concentration driven diffusion, the increase in ee cannot easily be explained in as much as the concentration driving force alone is considered to provide the permeation and enantioselectivity. We believe that the highly selective adsorption of the *S*-isomer results in high ee. Accordingly further works have been carried out with membranes prepared in NMP. The value of permeability co-efficient is lower in chiral polymer–DMF and chiral polymer–DMAc membrane and from this value we can conclude that NMP is perhaps the best solvent for preparing this type of chiral membrane.

### 3.5.2. Permeation rate and enantiomeric excess

The transport rate for both *S*- and *R*-enantiomer through chiral activated membrane, and the membrane enantioselectivity were investigated. The transport rate is expressed in terms of recovery percentage (*R*). The amount of chiral polymer in the membrane influences the recovery of racemic alcohol. The recovery percentage vs. time for 6 h experiment is shown in Fig. 7 from which it is apparent that, the recovery percentage of *R*-isomer increases with time whereas enantioselectivity as well as ee (%) was found to decreases. In such a case, the higher *R*-values were encountered when the amount of chiral polymer in the membrane was 10%. High amounts of chiral polymer in the membrane can lead to slightly denser membranes exhibiting higher resistance to transport through itself and consequently, a decrease in the transport rate of racemic alcohol was found. Although the presence of chiral polymer in the membrane facilitates the transport of racemic compounds, relatively high amounts of chiral polymer would tend to hinder it, probably due to the change in internal morphology of the membrane [36]. Therefore, the amount of chiral polymer is a critical parameter may be controlling the transport rate of the racemic alcohol.

Fig. 8 shows the normalized quantity ($Q_c$) of permeated (*R*)-isomer of *trans*-sobrerol vs. permeation time through chiral polymer–NMP membrane. All the polymeric membranes were amenable for enantioselectively separation of a racemic compound from an aqueous solution to give an (*R*)-isomer enriched

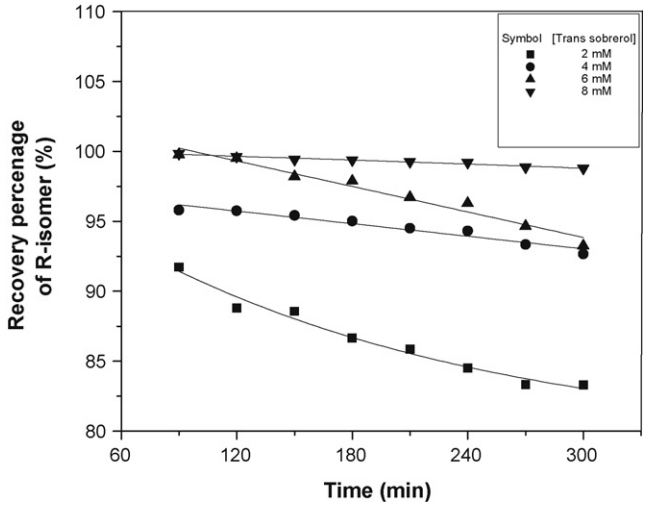


Fig. 7. Recovery percentage vs. time in different concentration of *trans*-sobrerol.

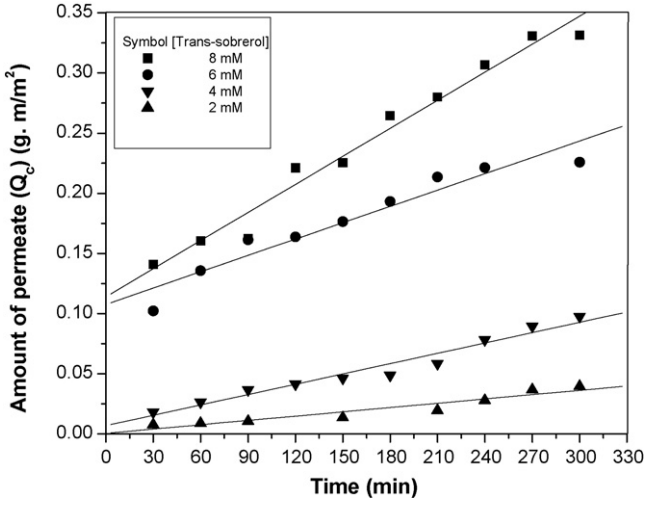


Fig. 8. Plots of quantity of permeated (*R*)-isomer ($Q_c$) in different concentrations of *trans*-sobrerol vs. permeation time through chiral polymer–NMP membrane.

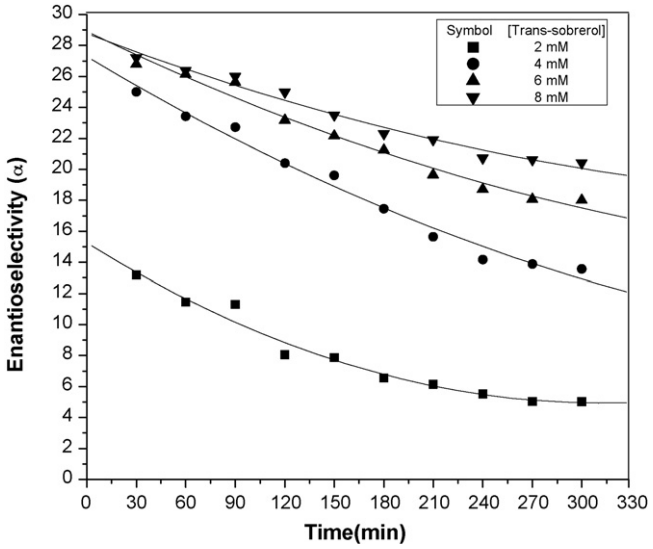


Fig. 9. Enantioselectivity vs. time in different concentration of *trans*-sobrerol.

permeate. Table 4 shows the enantioselectivity and permeation behaviour of *trans*-sobrerol through the chiral membrane. The chiral polymer–NMP membranes showed higher enantioselectivity than chiral polymer–DMAc and chiral polymer–DMF membranes, perhaps due to the formation of more uniform and regular microvoids in chiral polymer–NMP membrane.

As shown in Fig. 8 the permeation rate of *R*-isomer in terms of $Q_c$ increases with time as the concentration of the solution of racemic alcohol increases, as a result enantioselectivity and ee (%) increases with concentration but decreases with time (Figs. 9 and 10). This is perhaps due to the self-association of *S*-isomer on the chiral site of the membrane. The polymeric membranes we used showed (*R*)-isomer enantioselectively in permeation. This result directly indicates that the chiral main chain contributes to the enantioselective permeability. Aoki et al. [14] reported the enantioselective permeation of phenylalanine through depinanylsilylated polymeric membrane and the enantioselectivities through this membrane were lower than the original polymers. A membrane prepared by silylation of the backbone polymer provides helical conformation on the chiral zone and a molecular scale void, which enhances permeability of *R*-isomer as, reported in literature [16]. Hence, the importance of the contribution of the chiral main chain on enantioselective permeation was confirmed. Also, the silylated polymer of polyhydroxy containing phenylacetylene exhibited molecular scale voids that provides enhanced permeation rate for *R*-isomer of phenylalanine [17]. Molecular scale voids generated by depinanylation were retained and effective in enhancing the permeability values. Membranes from chiral poly(hydroxyl-containing phenylacetylene) exhibits higher permeability because of swelling effect in aqueous solution [17]. Siloxane-containing polymers are flexible and hence they are suitable for membrane application. Rigid structure is not suitable due to poor mechanistic integrity. For racemic *trans*-stilbene oxide, the enantioselectivity was favoured for *S*, *S* selectivity for this type of membrane. In our case enantioselective adsorption was occur and *S*-isomer was selectively adsorbed and heavy permeation of *R*-isomer becomes predominant. Thus selective adsorption or dissolution on the membrane surface may be the probable mechanism in our case.

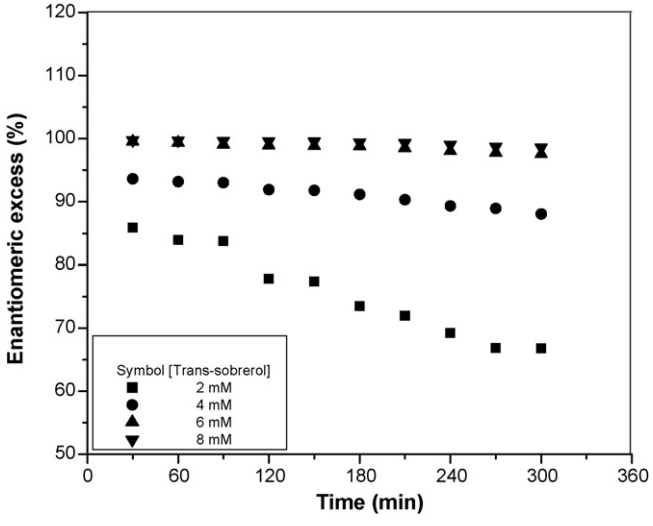


Fig. 10. Enantiomeric excess vs. time in different concentration of *trans*-sobrerol.

Figs. 9 and 10 also reveal that both the alpha values and the enantiomeric excess decrease due to the nonselective diffusion occurring after 6 h of the starting the experiment, which tends to equal the concentration between the two enantiomers in both aqueous phases. During the first 6 h experiment, the amount of *R*-enantiomer encountered in the permeate phase was always larger than that of *S*-enantiomer, implying that the *R*-enantiomer of the racemic alcohol transported across the membrane to the permeate phase. So the permeate solution is enriched in the *R*-enantiomer and consequently, the feed solution is enriched in the *S*-enantiomer. Thus, the free diffusion of the *S*-enantiomer from the feed to the permeate solution is favoured due to its higher concentration gradient between both aqueous phases.

Since the *S*-isomer was enantioselectively adsorbed, this selectivity behaviour may be opposite to that of permeation. Therefore, the permeation of *S*-isomer was thought to be suppressed by the relatively higher interaction with chiral polymer, resulting in the selective permeation of *R*-isomer which may be ascribed to the asymmetric carbons present in the chiral polymer. Further work to understand the controlling mechanism is in progress.

## 4. Conclusion

Chiral polymeric membranes were prepared by casting solutions containing polysulfone, chiral polymer and polyethylene glycol as additive with three different solvents like *N*-methyl-2-pyrrolidone (NMP), dimethylacetamide (DMAc) and dimethylformamide (DMF), separately using diffusion phase inversion method. From the polymer–solvent interaction point of view it was established that NMP is the preferred solvent for obtaining more uniform and regular surface morphology of the enantioselective membrane. The enantioselective membranes in three different solvents are tested for adsorption and

resolution of racemic alcohols. The *S*-isomer adsorbed mostly in chiral polymer–NMP membrane and follows Langmuir type of adsorption for all cases. Again, enantioselective permeation with higher enantiomeric excess value was obtained when NMP is used as the solvent, which is due to uniform and regular surface morphology in chiral polymer–NMP membrane. As the concentration of aqueous solution of recemate increases the enantioselectivity as well as enantiomeric excess increases up to a level of 98%.

## Acknowledgements

Financial support by Grant-in-Aid for Scientific Research from Department of Science and Technology, New Delhi is gratefully acknowledged. Useful discussion and suggestion of Dr N.N. Dutta, Scientist, NEIST-Jorhat is gratefully acknowledged.

## References

[1] R.D. Noble, Generalized microscopic mechanism of facilitated transport in fixed site carrier membranes, J. Membr. Sci. 75 (1992) 121–129.
[2] M. Ulbricht, Advanced 7 functional polymer membranes, Polymer 47 (2006) 2217–2262.
[3] J. Randon, F. Garnier, J.L. Rocca, B. Maïsterrena, Optimization of the enantiomeric separation of tryptophan analogs by membrane processes, J. Membr. Sci. 175 (2000) 111–117.
[4] M. Nakamura, S. Kiyohara, K. Saito, K. Sugita, T. Sugo, High resolution of DL-tryptophan at high flow rates using a bovine serum albumin-multilayered porous hollow-fiber membrane, Anal. Chem. 71 (1999) 1323–1325.
[5] N.H. Lee, C.W. Frank, Separation of chiral molecules using polypeptide-modified poly(vinylidene fluoride) membranes, Polymer 43 (2002) 6255–6262.
[6] M. Newcomb, R.C. Helgeson, D.J. Cram, Enantiomer differentiation in transport through bulk liquid membranes 96 (1974) 7367–7369.
[7] J.T.F. Keurentjes, L.J.W.M. Nabuurs, E.A. Vegter, Liquid membrane technology for the separation of racemic mixtures, J. Membr. Sci. 113 (1996) 351–360.
[8] A. Maruyama, N. Adachi, T. Takatsuki, M. Torii, K. Sanui, N. Ogata, Enantioselective permeation of (-amino acid isomers through poly(amino acid)-derived membranes, Macromolecules 23 (1990) 2748–2752.
[9] K. Shinohara, T. Aoki, E. Oikawa, Optical resolution by vapour permeation of 1,3-butanediol and 2-butanol through (+)-poly1-[dimethyl(10-pinanyl)silyl]-1-propyne membrane, Polymer 36 (1995) 2403–2405.
[10] T. Aoki, S. Tomizawa, E. Oikawa, Enantioselective permeation through poly[γ-[3-(pentamethyldisiloxanyl)propyl]-L-glutamate] membranes, J. Membr. Sci. 99 (1995) 117–125.
[11] T. Aoki, K. Shinohara, T. Kaneko, E. Oikawa, Enantioselective permeation of various racemates through an optically active poly{1-[dimethyl(10-pinanyl)silyl]-1-propyne} membrane, Macromolecules 29 (1996) 4192–4198.
[12] T. Aoki, Y. Kobayashi, T. Kaneko, E. Oikawa, Y. Yamamura, Y. Fujita, M. Teraguchi, R. Nomura, T. Masuda, Synthesis and properties of polymers from disubstituted acetylenes with chiral pinanyl groups, Macromolecules 32 (1999) 79–85.
[13] T. Aoki, Macromolecular design of permselective membranes, Prog. Polym. Sci. 24 (1999) 951–993.
[14] T. Aoki, M. Ohshima, K. Shinohara, T. Kaneko, E. Oikawa, Enantioselective permeation of racemates through a solid (+)-poly{{2-[dimethyl(10-pinanyl)silyl]norbornadiene}} membrane, Polymer 38 (1997) 235–238.
[15] M. Teraguchi, T. Masuda, Poly(diphenylacetylene) membranes with high gas permeability and remarkable chiral memory, Macromolecules 35 (2002) 1149–1151.
[16] M. Teraguchi, J. Suzuki, T. Kaneko, T. Aoki, T. Masuda, Enantioselective permeation through membranes of chiral helical polymers prepared by depinanylsilylation of poly(diphenylacetylene) with a high content of the pinanylsilyl group, Macromolecules 36 (2003) 9694–9697.
[17] M. Teraguchi, K. Mottate, S.Y. Kim, T. Aoki, T. Kaneko, S. Hadano, T. Masuda, Synthesis of chiral helical poly(hydroxyl-containing phenylacetylene) membranes by in-situ depinanylsilylation and their enantioselective permeabilities, Macromolecules 38 (2005) 6367–6373.
[18] K. Komura, N. nishitani, S. Itsuno, A novel approach to the synthesis of optically active poly(β-hydroxy carbonyl)s by aldol polymerization based on Mukaiyama Aldol reaction, Polym. J. 31 (1999) 1045–1050.
[19] L. Palacio, P. Pradanos, J.I. Calvo, A. Hernandez, Porocity measurements by a gas penetration method and other techniques applied to membrane characterization, Thin Solid Films 348 (1999) 22.
[20] K.J. Kim, A.G. Fane, Low voltage scanning electron microscopy in membrane research, J. Membr. Sci. 88 (1994) 103.
[21] A.G. Fane, C.J.D. Fell, A.G. Waters, The relationship between membrane surface pore characteristics and flux for ultrafiltration membranes, J. Membr. Sci. 9 (1981) 245.
[22] J. Marchese, C.L. Pagliero, Characterization of asymmetric polysulfone membranes for gas separation, Gas Sep. Purif. 5 (1991) 215.
[23] S. Hazarika, N.N. Dutta, P.G. Rao, A quantitative structure activity relationship study on permeation of amino acids in enantioselective membranes, J. Appl. Membr. Sci. Technol., in press.
[24] G. Capannelli, F. Vigo, S. Munari, Ultrafiltration membranes—characterization methods, J. Membr. Sci. 15 (1983) 289–313.
[25] H.M. Krieg, J. Lotter, K. Keizer, J.C. Breytenbach, Enrichment of chlorthalidone enantiomers by an aqueous bulk liquid membrane containing β-cyclodextrin, J. Membr. Sci. 167 (2000) 33–45.
[26] M. Mulder, Basic Principles of Membrane Technology, 2nd ed., Kluwer Academic Publishers, Dordrecht, The Netherlands, 2000.
[27] D. Stella, J.A. Calzado, S. Canepari, A.M. Girelli, R. Bucci, C. Palet, M. Valiente, Liquid membranes for chiral separations. Application of cinchonidine as a chiral carrier, J. Sep. Sci. 25 (2002) 229–238.
[28] R.D. Puts, D.Y. Sogah, Macromolecules 30 (1997) 6826.
[29] M. Muller, R. Zentel, Macromol. Chem. 194 (1993) 101.
[30] S. Hazarika, N.N. Dutta, S.D. Boruah, P.G. Rao, Proceedings of 9th National Conference of the Society for Polymer Science, India on Polymers for Advanced Technologies, Pune, India, December 17–20, 2006.
[31] Elipticity, $\theta$ = circular dichrosm $x$ 32,982, http://www.photophysics.com.
[32] S.I. Stoliarov, P.R. Westmoreland, M.R. Nyden, G.P. Forney, Polymer 44 (2003) 883.
[33] R. Guan, H. Dai, C. Li, J. Liu, J. Xu, Effect of casting solvent on the morphology and performance of sulfonated polyethersulfone membranes, J. Membr. Sci. 277 (2006) 148–156.
[34] B. Kruczek, Development and characterization of dense membranes for gas separation made from high molecular weight sulfonated poly(phenylene oxide). Effect of casting conditions on morphology and performance of the membranes, PhD thesis, University of Ottawa, Ottawa, 1999, pp. 29, 140–142.
[35] P. Overdvest, Enantiomer separation by ultrafiltration of enantioselective micelles in multistage systems, 2000, Promotoren: dr. ir. K. van't Riet, voormalig hoogleraar levensmiddelenpoceskunde.
[36] T. Gumí, M. Valiente, C. Palet, Elucidation of *SR*-propranolol transport rate and enantioselectivity through chiral activated membranes, J. Membr. Sci. 256 (2005) 150–157.